11-2022

Elastomer O-Ring Seal Swell Measurements for Sustainable Aviation Fuel Material Compatibility

Conor J. Faulhaber
University of Dayton

Elastomer O-ring Seal Swell Measurements for Sustainable Aviation Fuel Material Compatibility

Honors Thesis

Conor Faulhaber

Department: Mechanical and Aerospace Engineering

Advisors: Joshua Heyne, Ph.D. and Jamie Ervin, Ph.D.

November 2022

Elastomer O-ring Seal Swell for Sustainable Aviation Fuel Material Compatibility

Honors Thesis
Conor Faulhaber
Department: Mechanical and Aerospace Engineering
Advisors: Joshua Heyne, Ph.D. and Jamie Ervin, Ph.D.
November 2022

Abstract

As efforts continue to fight climate change by transitioning energy sources away from fossil fuels and towards renewable alternative, the commercial aviation sector finds itself at danger of falling behind in emissions reductions. To combat this, the best term opportunity to reduce the industry's contribution to greenhouse gas emissions has been identified as sustainable aviation fuel, or SAF, derived from renewable feedstocks like agricultural waste or used cooking oil. Currently, SAF is regulated to a 50%v blending limit with conventional petroleum-based fuel to maintain certain jet fuel properties, including material compatibility with elastomer o-ring seals. When these seals come in contact with conventional fuels, they absorb fuel and swell, creating a tight seal at junctions in fuel systems. O-rings have been found to not absorb SAF as proficiently due to low aromatic content, which is also known to contribute to sooting (and, consequently, higher emissions) during combustion. Thus, it is desirable to develop SAF that can induce sufficient o-ring swell while limiting aromatic content as much as possible. To make progress towards 100% drop-in compatible SAF, this study reviews relevant literature on the subject to inform experimental methods and designs. Optical dilatometry measurements, featuring a updated heated method, for seal swell are analyzed alongside the steric effects, molar volume, and density of a number of potential aviation hydrocarbons covering multiple hydrocarbon classes. Additionally, a linear volumetric blending rule is examined for this property and is used to develop a simple model for SAF blend property predictions centered around o-ring swell. The data gathered and property relationships identified in this study will aid in the advancement of SAF towards the 100% drop-in approval needed to meet industry and government goals for decreasing GHG emissions.

Acknowledgements

The author would like to acknowledge the immense amount of help and support for this research by the P.I. and effective Honors Thesis Advisor, Dr. Joshua Heyne, the stand-in Honors Thesis Advisor Dr. Jamie Ervin, and Dr. Samuel Dorf from the University of Dayton Honors Program. Without their assistance with administrative tasks, funding procurement, and technical advice this work would not be possible. Additionally, students Shane Kosir, Christopher Borland, Harrison Yang, David Bell, and John Feldhausen are owed credit for methods development, experimental assistance, and data provisions at various stages of this project. Lastly, Dr. Graham's contribution of 11 fuel samples to set a conventional swell range is highly appreciated. Funding was provided for this research from FAA Ascent Project 31 and the University of Dayton Honors Program.

University *of* Dayton

Table of Contents

Abstract **Title Page**

Introduction **1**

Climate change, aviation emissions, and SAF 1

Material compatibility with elastomer o-rings 1

Methods and Materials **4**

O-rings 4

Molecule selection 4

Fuels 7

Optical dilatometer hardware 7

Heated test method development 8

Software 9

Optical dilatometry experimental procedure 11

Results and Analysis **12**

Steric hindrance investigation 12

Initial blending rule study 13

Learning outcomes from initial studies 16

Fuel property relationships 15

Continuation of blending rule study 21

Development of potential SAF swell blends 23

Conclusions and Future Work **26**

Appendix A **28**

References **28**

1. Introduction

1.1. Climate change, aviation emissions, and SAF

In recent decades, global climate change has moved into the international spotlight as one of the great challenges of the 21st century, garnering the attention of policymakers, scientists, industry leaders, social justice groups, and the general public. The term "climate change" here refers to the disruption of temperature and weather patterns since the dawn of the Industrial Revolution caused mainly by the greenhouse gas emissions (GHG) released when humans burn fossil fuels [1]. This phenomenon has immense impacts on the environment, human health, global economies, and national security that are the subject of many research efforts [2]–[6]. The importance of this context as it pertains to the effects of the present work cannot be overstated, and for that reason a brief review of the direct motivation behind this study is provided.

The United States is targeting net GHG emissions reductions from 2005 levels by 50-52% by 2030 and 100% by 2050 [7]. Currently, transportation comprises the largest portion of the nation's GHG emissions at 27%, of which 8% are attributed to aviation [8]. With the electrification of ground transportation and the projected growth of the commercial aviation sector, this percentage is set to rise in the near future. In addition to its GHG contributions, commercial aviation also has direct effects on human health due to poor air quality from aircraft idling or taxiing [9], [10]. These concerns have brought about a large push for a more sustainable aviation industry via modernization of air traffic operations and technological advancements capable of handling the predicted rise in airborne transportation [11].

One of the most important technological advancements concerning the aviation industry deals with how aircraft are powered. For many of the reasons just described, it is desirable to move away from conventional petroleum-based fuels and towards sustainable alternatives. The three main alternative power sources potentially capable of filling this role are electric batteries, hydrogen fuel cells, and sustainable aviation fuel, or SAF. Of these options, SAF composed of synthetic hydrocarbons offers the best short-term opportunity to reduce aviation's GHG emissions because of its potential to fully replace conventional fuel without requiring major adjustments to current engine or aircraft hardware [11], also known as 'drop-in' compatibility. This potential has led to industry and governmental leaders in the United States to set specific goals to produce 3 billion gallons of SAF by 2030 and to fulfill 100% of U.S. aviation fuel demand with SAF (about 35 billion gallons per year) by 2050 [12].

1.2. Material compatibility with elastomer o-rings

A critical fuel science challenge in the 35-billion-gallon goal is how to meet drop-in compatibility with 100% synthetic hydrocarbons. SAF, per ASTM and FAA certifications [13], is limited to 50% blending with conventional fuel. The current blend limit is motivated by several factors, perhaps most notably material compatibility (specifically

here, o-ring swelling). When in contact with conventional jet fuels, o-rings absorb fuel, causing them to swell, which fills out the o-ring groove and maintains a tight seal at the connection point. The failure of elastomers within fuel systems to absorb SAF and sufficiently swell makes fuel systems prone to dangerous and wasteful loss of fuel, as seen in the fuel leakage during a NASA Glenn test campaign in 2011. This material compatibility issue, along with accurate fuel gauging via dielectric constant [14], remain as the key properties keeping aromatic molecules in aviation fuels.

Figure 1: NASA Glenn alternative fuel testing incident (2011)

The blend limit set to provide o-ring swelling was established partly to maintain aromatic content at approximately 8%v in any fuel blend containing SAF. Aromatics, which are not in currently commercialized SAF pathways (i.e., ASTM D7566 Annex 2 [15]), have historically been associated with providing the swelling needed and 'drop-in' compatibility. Aromatics, and their complementary property of seal swell, are also associated with higher non-volatile particulate matter (nvPM) emissions and, in turn, contribute higher radiative forcing in aviation via contrails [16], [17].

Important to understanding seal swell is the fact that it is a two-part process consisting of fuel absorption by the elastomer as well as the extraction of plasticizer by the fuel. The distinction between aromatic and paraffinic compounds remains the most telling molecular feature for seal swell. As mentioned, higher aromatic content, especially those with less and/or smaller alkyl branches, play a large role in the absorption of fuel [18], while n-alkanes tend to contribute more to the extraction process [19]. Iso-alkanes appear to have a negligible effect on either process [19], [20]. Cycloparaffins, and decalins in particular, have been identified as potential swell-inducing substitutes for aromatics, but to meet conventional swell levels they are required at higher concentrations [19]–[21] that may be unfeasible as an additive. Naphthalenes have also been identified as high-swelling compounds [18], but their high propensity for sooting makes them less desirable in fuel. To characterize a fuel's potential for sooting, a threshold sooting index (TSI) is derived

from smoke point measurements [22] or predicted from GCxGC-VUV compositional data. This allows SAF developers flexibility in including aromatics in fuels, as showcased by a 21/79%v SAK/HEFA (synthetic aromatic kerosene/hydrogenated esters and fatty acids) blend to power one engine of a United Airlines passenger flight on December 21st, 2021 [23]. The technical details of this fuel are fully investigated in the work of Feldhausen et al. [24].

To direct the search for specific swell-inducing molecules to replace aromatics, it is important to derive inter-property relationships. Though relatively limited in literature, some progress has been made in identifying molecular properties qualitatively associated with seal swell. A negative correlation between o-ring swell and molar volume is well documented [18], [20], [21], [25], [26], but this trend generally holds true only within hydrocarbon-type groups. For example, a paraffin will cause more swell than another paraffin of higher molar volume, but it will swell less than most aromatics regardless of molar volume. Other factors known to affect seal swell are molar mass, steric hindrance, and Hansen Solubility Parameters (HSP) [18].

The o-ring material has a significant influence on how the seal absorbs fuel. Aviation o-rings are typically composed of one of three materials: acrylonitrile-butadiene (nitrile rubber), fluorisilicone, and fluorocarbon. Of these materials, nitrile rubber seal swell is significantly more sensitive to compositional variance in jet fuel [19]–[21], [25], [26]. The higher swell consistency associated with fluorosilicone and fluorocarbon o-rings does not simply solve the material compatibility issue with SAF, however, because nitrile rubber offers considerable performance advantages in low-temperature scenarios [27]. Nitrile rubber material could theoretically be phased out of new aircraft and engine designs, but it would be difficult due to regulatory and logistical hurdles. Nitrile rubber's exaggerated impact on seal swell is both useful for investigating material compatibility and of high consequence to the industry, and, as a result, is the main focus of the analysis in this study.

Currently, there is no certified ASTM test method associated with measuring o-ring seal swell. Because of this, the experimental approach to quantifying seal swell varies through the literature between two main categories: material relaxation-based tests [19], [25] and optical measurements [18], [20], [21]. For both categories, a major impediment to the progress in this area of research is the duration of several days over which the fuel absorption process takes place. To integrate material compatibility into the regulatory approval process for jet fuels, it will be necessary to fully evaluate this property over the course of hours, not days. The current work employs the optical dilatometry technique described here and developed from works of Graham et. al and Kosir et al. [20], [21] because of its simplicity, cost-effectiveness, and the small amount of solvent required for testing compared to other test methods. Modest heating is shown here to accelerate the test without compromising the results, displaying an effort to bring testing times closer to those of other fuel properties.

To add to the relatively limited literature on this important fuel property, this study investigates seal swell as it relates to steric effects, molar volume, and density using binary blends of individual hydrocarbons and SAF. Additionally, the adherence to the linear volumetric blending rule proposed in Kosir et al. [21] is examined for individual dopants and then applied using a simple modeling technique to develop potential material compatible SAF blends. The results of this work will provide useful information to SAF developers for developing 100% 'drop-in' fuels in order to decrease the commercial aviation sector's contribution to GHG emissions.

2. Methods and Materials

2.1. O-rings

The two types of o-rings used in this study are acrylonitrile-butadiene (nitrile rubber or NBR) and fluorosilicone (FVMQ). All o-rings were manufactured by Parker Hannifin and were procured from Zatkoff Seals & Packaging. Unless otherwise noted, all o-rings tested for each type are all from the same manufacturing batch. This is important because the exact composition of aviation o-rings can vary between batches, changing the conventional swell range. While some fluorosilicone swell results are reported in this study, most of the results used for analysis are from nitrile rubber tests. This is because the NBR material is more sensitive to compositional changes in the test solvent/fuel, making it more useful for identifying patterns and a blending rule than FVMQ.

2.2. Molecule selection

To investigate the steric effects of individual hydrocarbons on seal swell, four shape-based groups were assigned to select molecules for testing. The four groups are 2D, 3D due to branching, 3D due to ring structure, and 3D by both branching and ring structure. These groups, while shape-based, inherently reflect the aromaticity of the molecules due to the effects of single and double bonds on molecule polarity. The eight hydrocarbon molecules that were selected for this study are listed in Table 1. These molecules were also used to evaluate a linear volumetric blending rule for seal swell for both FVMQ and NBR o-rings.

Table 1: Dopants and shape categories for steric hindrance study

Molecule	Purity	Molar Volume (mL/mol)	Shape Group
o-xylene	>98.0%	120.7	2D
acenaphthylene	>94.0%	169.5	2D
tetralin	>97.0%	135.9	3D Ring

n-butylcyclohexane	99%	175.5	3D Ring
propylbenzene	>99.0%	139.4	3D Branching
2-ethylnaphthalene	>99.0%	156.2	3D Branching
trans-1,3-dimethylcyclohexane	>95.0%	143.2	3D Both
tert-butylcyclohexane	>99.0%	172.6	3D Both

To build on findings from the steric hindrance study, thirty-nine chemicals, listed in Table 2 below, were doped at 8%v in C-1 Gevo and tested for seal swell. Of these molecules, there are 20 aromatics (14 alkylbenzenes, 2 cyclo-aromatics, 3 naphthalenes, and biphenyl), and 19 paraffins (16 monocycloparaffins, and 3 polycycloparaffins). Informed by the molar volume trend found in the literature, a focus was put on selecting smaller molecules in each hydrocarbon class as well as comparing results of aromatics to their substituted analogs. Halogenated compounds were ignored due to their lack of presence in most aviation fuels, and n-/iso-alkanes were not tested as dopant molecules here because of their lack of influence on seal swell. These tests are designed for comparison to the 8%v minimum aromatic requirement in jet fuel and are used to assess seal swell relationships with molar volume and density both across and within hydrocarbon classes.

Table 2: List of molecules used for larger property relationships study. Asterisks indicate an unconverged final swell value.

Molecule Name	Purity	Vendor	Density at 15°C [kg/m^3]	Seal Swell at 8%v in C-1 [%v/v]
alkylbenzenes				
benzene*	>99.8	Millipore Sigma	884.0	1.3
toluene*			869.0	3.8
ethylbenzene	>99.0	Honeywell	871.6	6
ortho-xylene	>98.0	TCI America	883.9	5.4
meta-xylene*	>99.0	TCI America	868.5	3.4
para-xylene	99	Alfa Aesar	866.7	4.7
n-propylbenzene	>99.0	TCI America	867.0	4.9
1,2,3-trimethylbenzene	>99.0	Sigma Aldrich	897.8	6.8
1,2,4-trimethylbenzene	>98.0	TCI America	879.7	5.1
1,3,5-trimethylbenzene	>97.0	TCI America	869.3	4.6
n-butylbenzene	>99.0	Acros Organics	865.1	3.9

n-pentylbenzene	96	Alfa Aesar	855.8	4.4
n-hexylbenzene	98	Alfa Aesar	863.6	4.3
n-heptylbenzene	>97.0	TCI America	862.1	3.1
cyclo-aromatics				
tetralin	>97.0	TCI America	973.6	6.8
indane	>95.0	TCI America	967.5	8.3
naphthalenes				
1-methylnaphthalene	>98.0	TCI America	1023.8	15.0
2-ethylnaphthalene	>99.0	TCI America	996.8	12.1
2-isopropylnaphthalene	>95.0	TCI America	975.3	10.9
biphenyl				
biphenyl	99	Alfa Aesar	1041.0	17.4
monocycloparaffins				
cyclohexane	>99.0	Fisher Chemical	784.2	2.0
methylcyclohexane	99	Sigma Aldrich	769.4	1.6
ethylcyclohexane	>99.0	Acros Organics	794.2	1.9
cis-1,2-dimethylcyclohexane	>98.0	TCI America	802.4	1.0
trans-1,2-dimethylcyclohexane	>99.0	TCI America	781.5	1.2
cis-1,3-dimethylcyclohexane	>99.0	TCI America	773.0	0.4
trans-1,3-dimethylcyclohexane	>95.0	TCI America	789.4	1.0
cis-1,4-dimethylcyclohexane	>98.0	TCI America	788.5	1.0
trans-1,4-dimethylcyclohexane	>95.0	TCI America	768.8	1.2
n-propylcyclohexane	>98.0	TCI America	793.8	
1,2,4-trimethylcyclohexane	>96.0	TCI America	785.8	1.0
1,3,5-trimethylcyclohexane	>98.0	TCI America	778.9	1.0
n-butylcyclohexane	99	Alfa Aesar	804.0	1.0
n-pentylcyclohexane	98	Alfa Aesar	807.0	1.5
n-hexylcyclohexane	>98.0	TCI America	812.0	0.5
n-heptylcyclohexane	>99.0	TCI America	805.3	1.0
polycycloparaffins				
cis-decalin	>98.0	TCI America	900.7	1.7
trans-decalin	>98.0	TCI America	873.7	1.9
bicyclohexyl	>99.0	TCI America	890.3	1.0

Additionally, n-butylcyclohexane, propylbenzene, tetralin, 2-ethylnaphthalene, and propylcyclohexane are used to verify the linear blending rule over a wide range of dopant concentrations in Gevo C-1. The success of the blending rule is measured using an r^2 value of the linear trendline through the data points for each molecule.

2.3. Fuels

11 different shipments of conventional jet fuel provided by Dr. John Graham of UDRI, along with an additional sample of A-2 from the NJFCP program [28], were used to set a 3 standard deviation conventional jet fuel range for seal swell. Because of compositional variance between manufacturing batches of nitrile rubber o-rings [27] it is necessary to reestablish the conventional swell range for each batch received. The 3 standard deviation range for conventional jet fuel swell tested with the batch of o-rings used in this study is 9.2%-16.6%v/v.

Two SAFs, C-1 Gevo ATJ and World Energy HEFA (hydroprocessed esters and fatty acids), approved by the FAA for up to 50%v blends in conventional jet fuel were used in this study. These fuels are made up of mainly n- and iso-alkanes, and thus exhibit very low swelling. Their insufficient swell characteristics and industry approval make these SAFs useful for both identifying swell-inducing molecules and showcasing potential dopant blends that can bring low-swelling fuels up to the conventional swell range. Lastly, the 21/79%v SAK/HEFA blend studied in Feldhausen et al. [24] is included in this study as an example of a SAF that meets ASTM D7566 specifications and conventional seal swell levels. Relevant details regarding these fuels are listed in Table 3 below.

Table 3: List of specific fuels referenced in this study. SAK/HEFA data is pulled from Feldhausen et al. [24]

Fuel Name	POSF	Producer	Molar Volume [mL/mol]	Density at 15°C [kg/m^3]	Neat Seal Swell [%v/v]
A-2	10325	Shell Mobile	198.9	803.5	13.7
C-1	13718	GEVO	237.4	759.3	0.5
HEFA	n/a	World Energy (WE)	214.3	751.4	0.3
SAK/HEFA 21/79	n/a	Virent/WE	150.4	776.1	12.3

2.4. Optical dilatometer hardware

The optical dilatometers (ODs) used here are custom built using optical stand materials procured from Thor Labs. There are three main components to the dilatometer: a camera, an optical stage, and a light source. The camera is an Allied Vision Alvium 1800 U-500m, 1/2.5" 5.0MP C-Mount, USB 3.1 Monochrome Camera equipped with a 35mm, f/16 Ci Series Fixed Focal Length Lens. Set about 6 inches above the camera lens is the optical stage, which consists of a ring stand with a 3” x 1” glass microscope slide placed on top for the vial containing the solvent and o-ring sample to rest. 2-3” above the vial sits the light source, which is a YGS-Tech 2 Inch LED Recessed Lighting Dimmable Downlight, 4000K Natural White purchased from Amazon.com and provides ample lighting for the image processing software to identify the o-ring sample in the photos. The entire OD is

mounted to a Thor Labs Optical Breadboard to reduce the risk of vibration on the test sample. The diagram in Figure 2 below depicts this dilatometer set up.

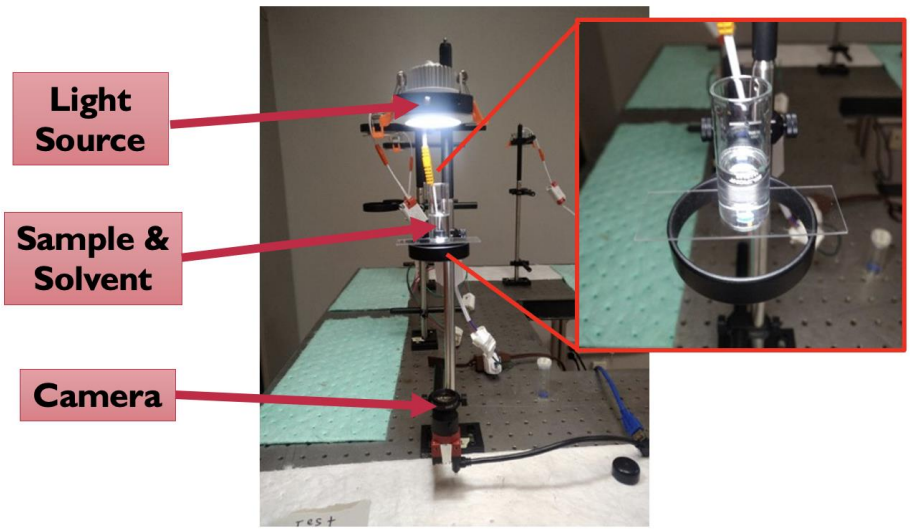

Figure 2: Basic dilatometer set-up

2.5. Heated test method development

After about a year of duplicating this OD setup to increase testing capacity, it became desirable to shorten the actual duration of the test while still observing converged o-ring swelling. This led to the development of a custom-built oven with optical dilatometry hardware integrated into the structure of the oven itself, creating a heated environment to increase the diffusion rate of the solvent into the o-ring material. The oven is designed to operate at around 37°C, about 10°C above ambient room temperature but remaining below the 38°C flashpoint limit for aviation fuel. Test time until convergence inside the oven is generally reduced by up to half the time until convergence of tests run at room temperature.

The first iteration of the oven was built using a wooden frame, simple 3/8" thick foam insulation panels on the sides and top, and non-optical glass as the stage. It consisted of 8 dilatometers and was heated using a simple duct system with a space heater hooked up to a temperature controller. As a proof of concept, this design was successful in speeding up tests, however the cheaper materials eventually began to fail and the heater was prone to unwanted shutoffs, so it was necessary to build and design a more robust heater of the same size while incorporating two more dilatometers.

The structure of the oven was built using 80/20^{TM} aluminum framing and plastic paneling materials and is about 4' wide, 1.7' tall, and about 1.5' deep. 2.5" thick Kingsguard GreenGuard Foam Board was cut to fit within the frame to insulate the panels on each side, except for the bottom. Five equally spaced holes, each slightly less than 1" diameter, were drilled into each of the two bottom panels for the dilatometer stages, which consist of microscope slides cut to 1" squares securely taped over the holes inside of the

oven. The top panels, as well as the top foam boards, have five ~3" holes for the LED lights and coincide with the stage holes on the bottom panel. The entire oven structure is mounted on a Thor Labs Optical Breadboard so that the camera can be mounted under each stage.

The heating elements for the oven are two adhesive thermal pads from Tutco Heating Solutions with customized holes for each dilatometer stage to provide optimum heating around each test. Each pad is wired to a standard wall plug and draws 120W. A controller was also purchased from Tutco and is used to set each heater slightly above the desired temperature of 38°C to offset the heat loss through the uninsulated floor of the oven. The amount to which this must be offset depends on the temperature of the lab environment, and a thermometer set inside of the oven is used to monitor the actual oven temperature. The full specifications of these heating pads can be found in Appendix A. The current testing capacity of this work consists of 13 total dilatometers, 10 heated in the newer oven and 3 unheated using the original dilatometer design described above.

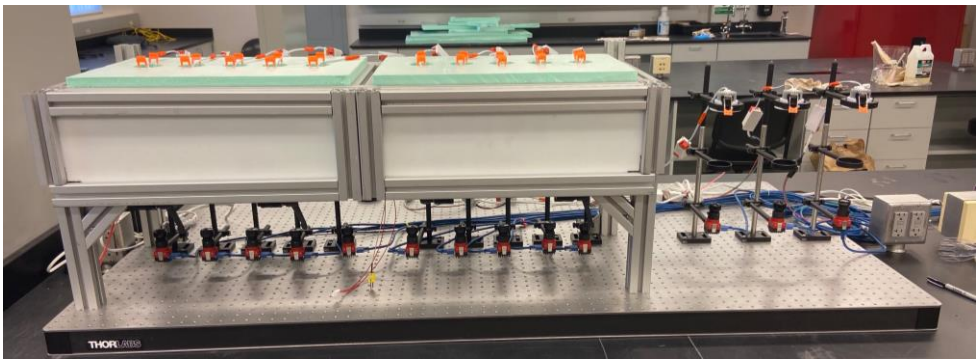

Figure 3: Current dilatometer set-up with 10 heated tests in the oven and 3 unheated stands.

2.6. Software

2.6.1. Image capture

Optical dilatometry measurements of seal swell are outputted as raw data in the form of hundreds of photographs taken at 10-minute intervals. To gather these images, a custom software was developed by a former colleague, University of Dayton graduate Shane Kosir, using Pymba, the Python wrapper for Allied Vision's Vimba C API, which is the compatible software for the cameras used on the optical dilatometers. Using a separate instance of the code for each camera, photos are taken at every 20 seconds to be used for linear regression to the actually test start time, and then every 10 minutes after the tenth photo is taken. The photos are all saved into a single subfolder in within test's folder containing all the necessary code and data gathered. The naming convention of the photos includes the time of the photo taken, initially based on test time but updated to absolute time in the most recent method, to be used for analysis of swell over time.

2.6.2. Image processing

To convert the raw images into useful data points, image processing software is required. The open-source software package ImageJ, developed by Wayne Rasband and the NIH was first employed for this purpose. To acquire the area measurements, "binary", or black and white, images are first manually loaded into the software. Then, the operator designates a threshold that separates the object of interest, in this case an o-ring sample, from the background. After selecting the area containing the o-ring, the images are analyzed. This consists of the software counting all of the pixels both within the threshold range and the selected area, and outputting a .csv file consisting of the area of the o-ring in each picture in pixels. More information on this software is available at the software's download and wiki websites [29], [30].

Due to the expansion in testing capabilities by the addition of dilatometers and development of faster, heated tests, it became necessary to automate the image processing software. A custom, Python-based image processing software was developed by a colleague on the project, University of Dayton student Christopher Borland, to accomplish the same task as ImageJ with less manual inputs. While using the same general method of threshold-setting and pixel-counting, this program combined the processes of automated picture taking and image processing into one action. Each time a picture is taken, the software uses Artificial Intelligence to locate the o-ring and uses a constant threshold to measure area in pixels in a similar manner to ImageJ. Tests comparing the updated method to ImageJ results for the same set of photos exhibits negligible differences in pixel area, meaning that more recent results can be compared to results using the older method. This software also automatically updates a log of tests and records the picture start time, in seconds, that can be easily referenced in the swell calculation code and enables more efficient data organization.

2.6.3. Swell calculation

After the .csv file for a test is generated, the actual volume swell of the o-ring must be calculated from the area data. To obtain the true initial o-ring size, the SciPy Stats Python package is used to perform a linear regression on the first 10 data points using the picture start time, which is obtained by starting a stopwatch at the moment the solvent touches the o-ring sample and stopping it as the image capture code begins. Using this initial o-ring size, Equation 1 is applied to each area value to calculate a swell volume percent, V_i, at the time extracted from the corresponding photo's file name.

$$V_i = \left(1 - \frac{A_i}{A_0}\right)^{3/2} * 100 \qquad (1)$$

A_0 and A_i are the areas of the o-ring when it is first submerged and at the desired time of swell measurement, respectively. The reported swell is calculated using the average o-

ring surface area of the last 30 pictures collected. It is assumed that the o-rings swell isotropically.

These calculated values are the final version of the data that is used for all analysis and determination of test convergence. The most recent iteration of the swell calculation process features the ability to get swell results for multiple tests simultaneously, the automation of swell vs. time plotting, and easier data formatting to reduce the post-processing needed for analysis.

2.6.4. Plotting and data analysis

All of the analysis for this study was conducted using Python in some form, with some data organization being provided by Microsoft Excel. The Pandas and NumPy packages were used in tandem with .csv or Microsoft Excel notebooks for data formatting and simple calculations. The package SciPy Stats was used for more advanced calculations like linear regressions and r^2 values. Matplotlib in Python was employed to generate plots for data visualization that allowed for the identification for patterns and trends in the data as well as an appealing presentation of the results.

Additionally, a simple model for determining potential SAF blends was developed using Microsoft Excel. The model is built around selecting a desired density, which in the case of this study was the ASTM D7566 minimum for jet fuel, 775 kg/m^3. Using swell, molecular weight, density, TSI, and dielectric constant property data for six molecules and a given SAF the model projects three-part blends (two molecule dopants and SAF) at different volume ratios that meet the set density. Using these ratios, the model then predicts the aforementioned properties for each blend using known or proposed blending rules. Then, the data is filtered for blends that meet specification or conventional range for all or most properties. The blends are then mixed, tested, and the measured results are compared to the predictions.

2.7. Optical dilatometry experimental procedure

Using the equipment and software described in detail above, the procedure for performing seal swell measurement using this test method is as follows: First, using gloves suited for contact with fuels, a 10mL glass vial and cap are cleaned using acetone or deionized water and are thoroughly dried and inspected for any smudges, dirt, dust, or leftover fluids that will either inhibit clear pictures from being taken or contaminate the solvent. Then, an o-ring cross-section is cut by hand using a scalpel or razor blade. The ideal o-ring sample is as thin as possible while maintaining the appearance of a perfect cylinder. The quality of the sample is then checked by placing the o-ring into the vial, setting it on the dilatometer stage, and running a simplified acquire image code to capture an “initial image” used to assess the uniformity of the sample. When this is verified, the sample is removed from the vial and placed in a clean and dry petri dish using forceps. Then, the desired solvent(s) are deposited into the vial, using a pipette to measure 5mL of

total solvent. If multiple solvents are being blended, the cap is placed on the vial and the vial is shaken until thorough blending is achieved. The solvent should remain capped until the image capture software is properly set-up for the test. Once this is done, and the computer operator is ready, the o-ring sample is to be dropped into the vial as the computer operator simultaneously begins the picture start timer. Then, the o-ring sample is adjusted to the center of the vial to avoid the distortion around the edges, and the vial is placed onto the dilatometer stage. This is when the computer operator can finish the image capture prompt sequence, and the test will continue as automated.

Room temperature tests typically run for 10-14 days before convergence, though some tests can last over a month. Heated tests typically run for 5-10 days. Convergence is observed when the swell value remains relatively unchanged for over 24 hours. To check this, the swell calculation software is run every 1-2 days to monitor the progression of swell and confirm proper data collection. Once a test is converged, the image capture/processing code is stopped, the swell calculation software is run one more time, and the results are collected for analysis. Then, the solvent and sample are both discarded in their proper waste containers and all glassware is cleaned. Though it has not been employed here yet, future tests may utilize GCxGC-VUV analysis on the solvent before and after swell measurement to investigate the change in composition after interaction with the o-ring.

3. Results and Analysis

3.1. Steric hindrance investigation

Figure 4 displays nitrile rubber swell measurement results for the steric hindrance study as they relate to the molar volume of the dopant molecule. NBR in solvents containing molecules in the 3D Ring and 2D shape categories exhibited expected behavior, swelling higher for molecules with lower molar volumes and vice versa. Dopants in the 3D Both category induced very low volume swell regardless of molar volume, and those in the 3D Branching category appeared to show a positive correlation between swell and molar volume. This is likely due to the fact that while these two molecules, 2-ethylnaphthalene and propylbenzene, are related by their general shape, naphthalenes are known to exhibit higher swelling than alkylbenzenes. This indicates that the shape categories used here to generalize hydrocarbon classes likely do not accurately characterize o-ring swell.

Only three nitrile rubber tests produced swell results within the conventional swell range: o-xylene at 15% concentration and tetralin at both 15% and 10% concentrations. Two other tests, propylbenzene at 15% concentration and 2-ethylnaphthalene at 10% concentration, swelled within 0.3% v/v of the conventional minimum and maximum limits, respectively. Notably, all five of these tests are with aromatic molecules at concentrations around those found in conventional jet fuel, except for 2-ethylnaphthalene, which is limited to 3% concentration by volume by ASTM D7566. The lack of non-aromatic molecules producing sufficient swell is motivation for a more detailed study of seal swell over a wider range of aviation hydrocarbons.

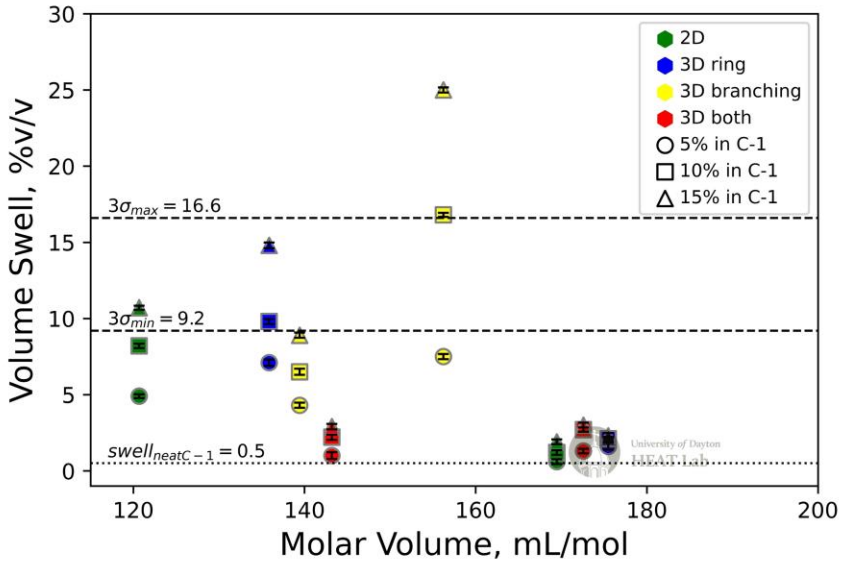

Figure 4: O-ring swell for NBR by shape category with molar volume and molecule concentration in C-1. The conventional swell range is indicated by dashed lines and neat C-1 volume swell is shown by the dotted line

Every molecule caused positive volume swell for NBR relative to the swelling from neat C-1. NBR tests showed increased swelling with concentration in all cases; however, the amount of swelling between different concentration levels varied in magnitude between molecules.

3.2. Initial blending rule study

Figure 5 shows the linearity of volume swell of NBR and FVMQ for 2D, 3D Ring, 3D Branching, and 3D Both molecule shape categories. For a given material and molecule at different concentrations a linear trendline was fit to the data, including the swell measurement for neat C-1 with the appropriate material. Linearity was measured using the r-squared value of each series of tests and signifies the current predictability of the swelling caused by the molecule.

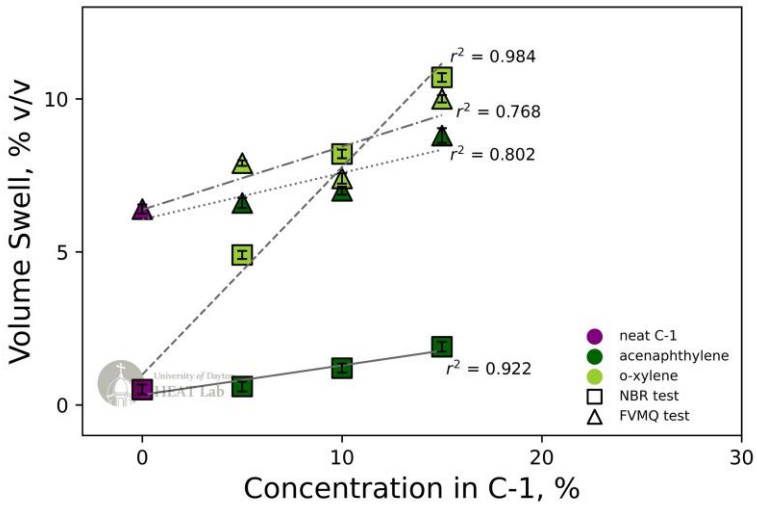
Volume Swell, % v/v
Concentration in C-1, %
r^2 = 0.984
r^2 = 0.768
r^2 = 0.802
r^2 = 0.922
neat C-1
acenaphthylene
o-xylene
NBR test
FVMQ test
University of Dayton
HEAT Lab

(a)

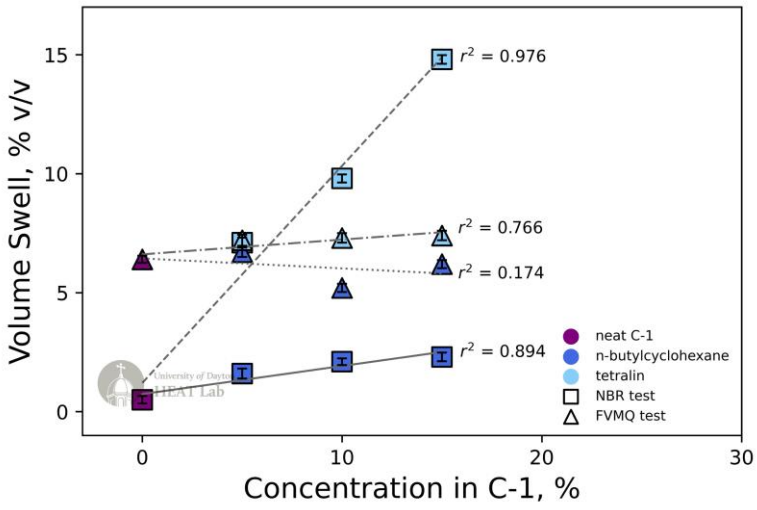
Volume Swell, % v/v
Concentration in C-1, %
r^2 = 0.976
r^2 = 0.766
r^2 = 0.174
r^2 = 0.894
neat C-1
n-butylcyclohexane
tetralin
NBR test
FVMQ test
University of Dayton
HEAT Lab

(b)

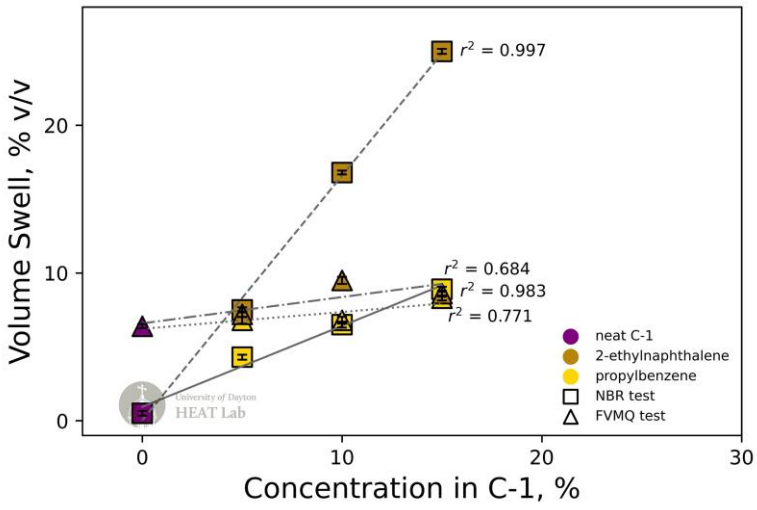
Volume Swell, % v/v
Concentration in C-1, %
r^2 = 0.997
r^2 = 0.684
r^2 = 0.983
r^2 = 0.771
neat C-1
2-ethylnaphthalene
propylbenzene
NBR test
FVMQ test
University of Dayton
HEAT Lab

(c)

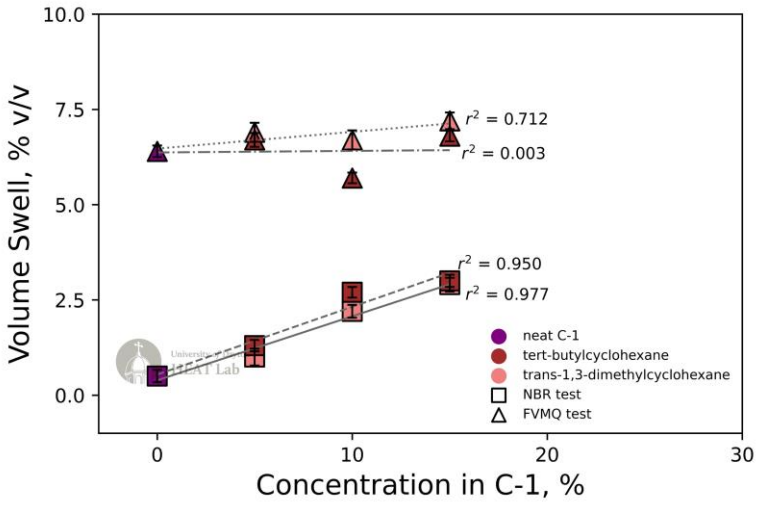

(d)

Figure 5: Volume swell of NBR and FVMQ with molecule concentration for molecule shape groups (a) 2D (b) 3D Ring (c) 3D Branching (d) 3D Both with linear trendlines and r^2 values for each series of tests

For NBR, the highest linearity was exhibited by 2-ethylnaphthalene (r-squared value of 0.996), and the lowest linearity was shown by acenaphthylene (r-squared value of 0.614). Generally, the molecules that induced higher swell tended to show higher linearity in swelling with concentration. Of the four molecules within or close to the conventional swell range for NBR, the lowest r-squared value was for tetralin at 0.981, indicating that these molecules swell NBR o-rings both predictably according to a linear blending rule and sufficiently at the concentrations shown in Figure 4

Both n- and tert-butylcyclohexane exhibited a non-increasing swelling trend with concentration for FVMQ as shown in Figures 3(b) and 3(d). Compared to NBR, FVMQ exhibited far more unpredictable behavior in the form of nonlinearity between volume swell and molecule concentration and shrinking of the o-ring sample.

Interestingly, acenaphthylene, which displayed the lowest linearity for NBR, had the highest linearity for FVMQ (r-squared value of 0.802), while swelling from n-butylcyclohexane (r-squared value of 0.003) was almost entirely unpredictable for this material based on a linear blending rule. Unlike NBR, the amount of swelling induced by the molecule did not significantly affect the linearity of the swell; however, both molecules that displayed non-increasing volume swell with concentration (n- and tert-butylcyclohexane) had drastically lower r-squared values than the rest (0.003 and 0.174, respectively).

Non-aromatic molecules were generally more unpredictable based on a linear blending rule, meaning that even if a non-aromatic molecule was found to induce sufficient volume swell for NBR, it could potentially under- or over-swell an FVMQ o-ring even at controlled concentrations.

3.3. Learning outcomes from initial studies

The results from the steric hindrance study failed to clearly characterize o-ring swelling based on steric effects and molar volume, and no suitable molecules were identified as potential SAF dopants to induce seal swell without dramatically increasing aromatic content. The blend rule study showed reasonable accuracy to the linear blending, especially for NBR, but the small range of concentrations are a cause for further investigation. Despite these shortcomings, this work gave valuable guidance the next phase of swell measurements. The mixed results from these tests made it apparent that a much wider range of molecules should be selected for measurement and comparison at a single concentration. The selection of these molecules was also refined, using the suggestion of relatively low branching hydrocarbons from Romanczyk et. al. [18] and the removal of molecules that are unlikely to be used in jet fuel (i.e., acenaphthylene) from analysis. Instead of using relatively arbitrary shape categories for comparison, relevant molecular properties for the blends (as opposed to properties of only the dopants) and hydrocarbon classes should be the focus of the study. Additionally, the blending rule should be verified for higher concentrations. To accomplish these testing goals, the aforementioned improvements in testing efficiency were implemented and the experimental design changes suggested here were applied. Lastly, this study proceeds using only NBR o-rings as their sensitivity to fuel composition shows the nature of o-ring swelling more clearly in the results.

3.4. Fuel property relationships

Figure 6 shows the seal swell over two weeks of testing for the molecules listed in Table 1 doped at 8%v in C-1, allowing for the comparison of the experiments that did not converge (benzene, toluene, and m-xylene) to the rest of the runs by the progression of swell rather than by the swell value at the time of convergence. Runs are marked using a colorbar normalized by one of two properties: molar volume or density. This was done to compare the well-documented seal swell relation with molar volume to that with density, which was used here to characterize the structural differences between hydrocarbon classes (# of rings, H/C ratio, etc.) that affect how tightly atoms are packed into a molecule.

The volume fraction of dopant in low-aromatic SAF is intentional so that these results can be compared to the 8%v aromatic requirement achieved by blending SAF with +50%v of conventional jet fuel. For the same reason, the properties are reported for the entire mixture rather than the dopant itself, which is especially meaningful as it relates to the ASTM D7566 required density range (775-840 kg/m^3). Also, though reporting mixture properties is more useful to the industry, it should be noted that because C-1 is used at the same volume fraction in all tests reported in this section, it is the dopant molecules driving the difference properties for the mixture.

Figures 6(a) and 6(b) show the relationship between molar volume and seal swell. While roughly apparent for paraffins, the negative molar volume trend documented in the literature is shown clearly within the alkylbenzenes tested. However, the molar volumes of these mixtures do not distinguish the hydrocarbon class of the dopants from each other.

This contrasts with the positive swell trend with density as the alkylbenzenes in Figure 6(c), as a class, are denser and swell more than the paraffins in Figure 6(d), making density more suitable to describe seal swell when looking at the entirety of hydrocarbon classes. Molar volume remains a useful indicator of seal swell, though, because of its relationship within hydrocarbon classes. Polycycloparaffins are especially interesting considering their densities resemble that of an aromatic while they perform more similarly to monocycloalkanes in swell tests.

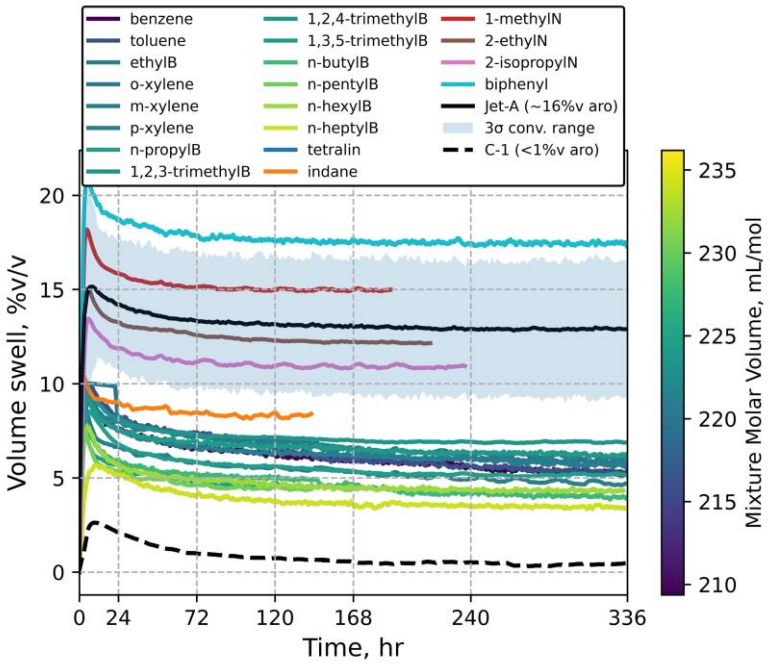

(a) Aromatics colored by mixture molar volume

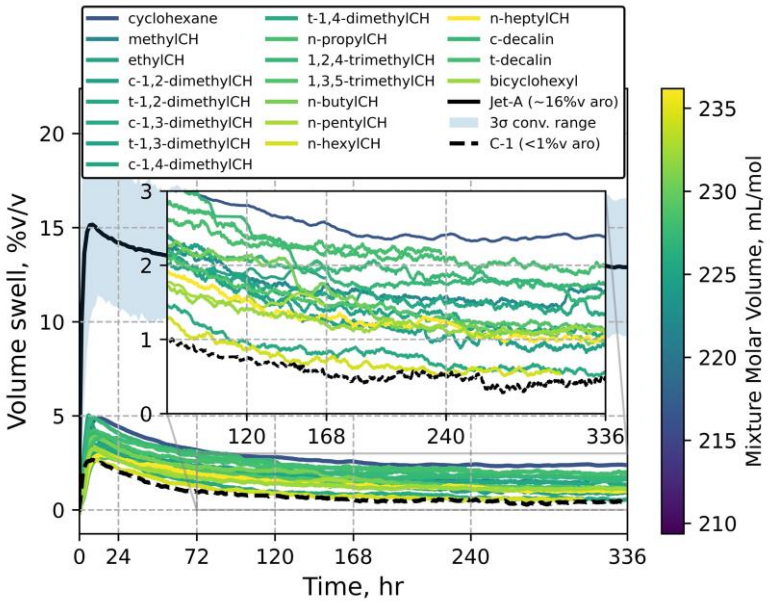

(b) Paraffins colored by mixture molar volume

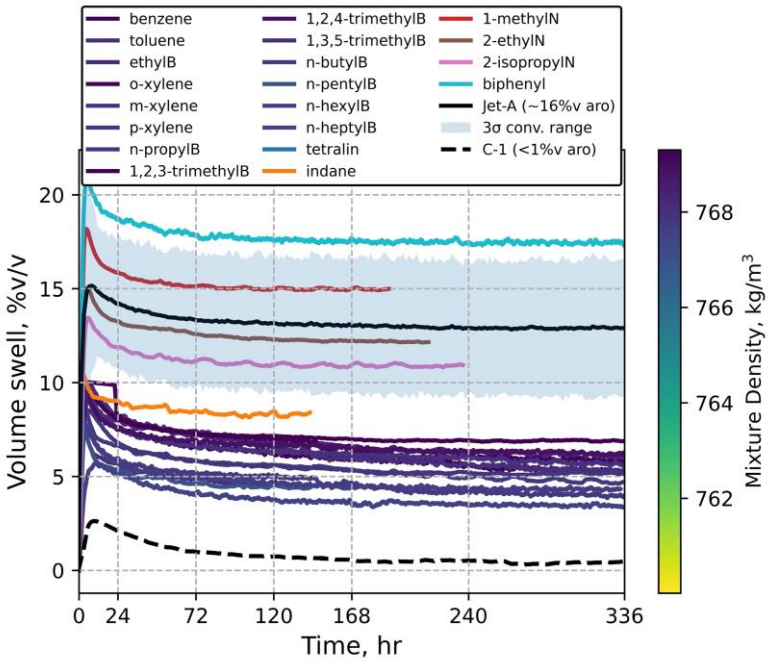

(c) Aromatics colored by mixture density.

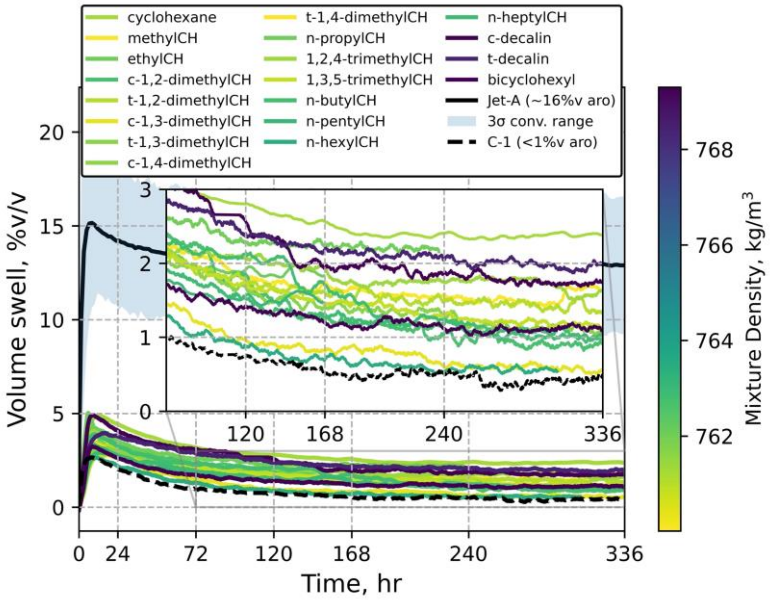

(d) Paraffins colored by mixture density

Figure 6: O-ring seal swell over time for aromatic and paraffinic molecules doped at 8%v in C-1. Subplot captions indicate molecules depicted and the property used to color each test.

To further illustrate these property trends, Fig. 7 contains scatter plots of the converged swell results of the materials shown in Fig. 6 as well as HEFA, C-1, A-2, and blends of the latter two fuels at ratios of 50/50%v and 25/75%v, respectively. With molar volume, the

swell results separate into “tiers” designated by the aromaticity of the mixture. Inside each “tier” appears the known negative seal swell relationship, but the intensity of this effect varies between classes. For density, a clear positive correlation over all mixtures is apparent, apart from polycycloparaffins.

Although their behavior is not completely understood, cis- and trans-decalin may prove useful to SAF developers because low-aromatic, alkane-rich SAFs often fail to meet the minimum density requirement for jet fuel. Low density n- and iso-alkane molecules, though not swell inducing, are desirable for SAFs because of their small contributions to nvPM emissions. As such, it is advantageous to maintain relatively high n- and iso-alkane volume fractions in the final product while ensuring compatibility with o-ring seals. Decalin is a possible blend component that increases both swell and mixture density more efficiently than most other paraffins while maintaining a low contribution to the overall emissions of the fuel

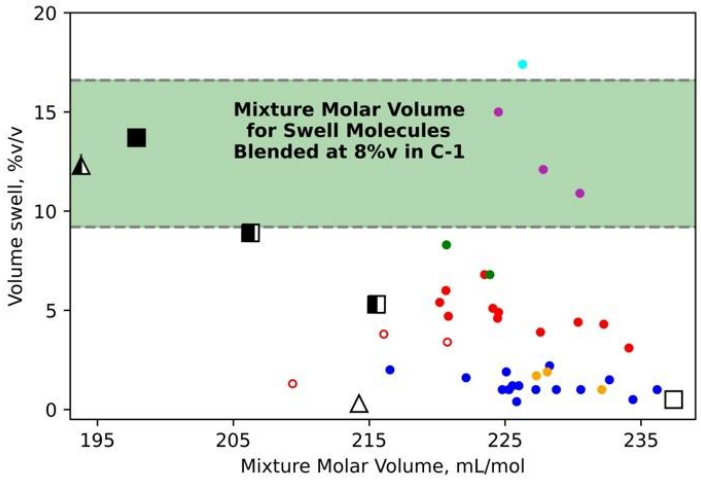

(a)

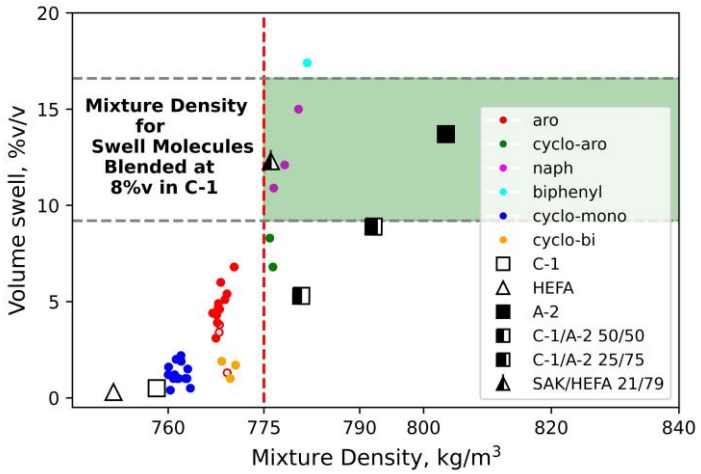

(b)

Figure 7: Scatter plots depicting the final o-ring swell for each molecule doped at 8%v in C-1 compared to the molar volume (a) or density (b) of the mixture. Empty circular markers represent the tests in this study whose swell did not converge. The gray dashed lines represent the limits of the conventional swell range and the red dashed line in (b) is indicative of the ASTM D7566 minimum density specification.

Of note in Fig. 7 is that of the dopants tested at 8%v in C-1, only the naphthalenes induced swelling within conventional swell range. The alkylbenzene-doped mixtures here are reflective of a need for a swell measurement-based standard for material compatibility, as 8%v aromatic content does not necessarily imply adequate seal swell. The C-1/A-2 blends shown here also showcase the limitations of the 8%v aromatic requirement, as even a blend ratio of 25/75%v does not meet the minimum conventional swell. In other cases, such as the SAK/HEFA blend, aromatics are utilized well above 8%v to meet conventional swell while maintaining a TSI below that of conventional fuel [24].

Out of the molecules doped at 8%v in C-1, only biphenyl, napththalenes, and cycloaromatics brought the mixture density within the ASTM specification range. Additionally, blending C-1 in A-2 at the 50%v blend limit results in a mixture density within the specification range by a relatively small margin. Given the potential for variation in properties between production batches of fuels [31], this indicates that conforming C-1/petroleum fuel blends frequently contain less than 50% C-1 because they can be limited by density, the 8%v aromatics requirement, or some other D7566 requirement even when not limited by C-1 product availability or cost.

Addressing the discrepancies between measured conventional seal swell and that caused by the 8%v aromatic requirement is essential to increasing the usage of SAF in commercial aviation. Property-based relationships including, but not limited to, those discussed in this work are needed to accurately project material compatibility for neat fuels as well as blends due variability composition between novel SAFs. Important to this is quantifying the relationship between molecule concentration and seal swell across hydrocarbon classes.

3.5. Continuation of blend rule study

The relationship between seal swell and concentration was studied using 4 molecules, n-butylcyclohexane, n-propylbenzene, tetralin, and 2-ethylnaphthalene, doped at 5%v, 8%v, 10%v, 15%v, 25%v, and 40%v in C-1. Seal swell is plotted in Fig. 8 at 1-, 3-, 7-, and 10-day timesteps when available for each molecule, in addition to the converged measurements. The results for each timestep are characterized by a linear trendline with a reported r^2 value to show the validity of a linear blending rule over the duration of the swelling process. The results for tetralin and 2-ethylnaphthalene at 25%v and 40%v are not shown because their extremely high swell made the trendlines indistinguishable from each other and the r^2 value changed minimally without these data points.

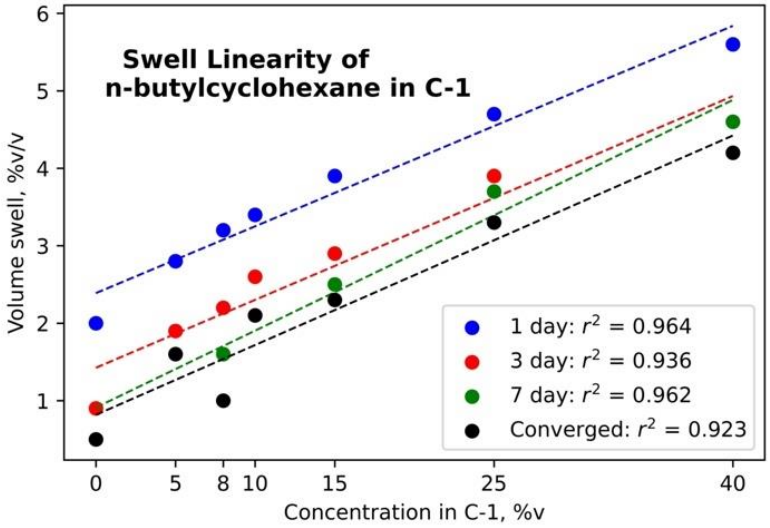

(a)

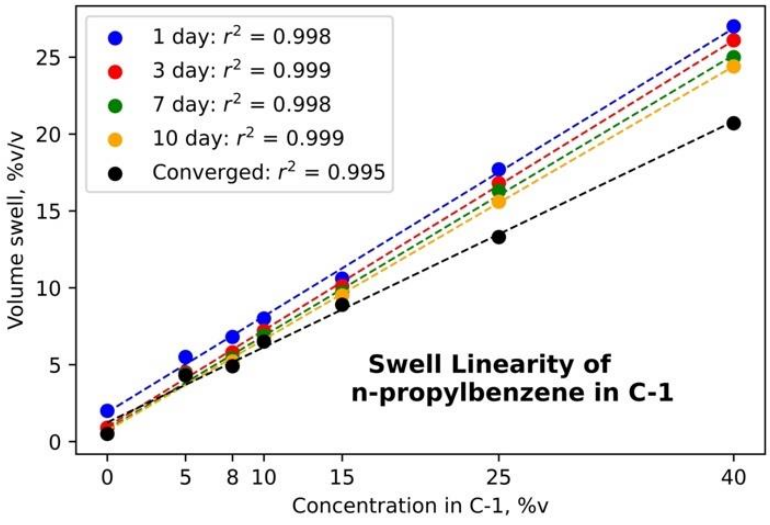

(b)

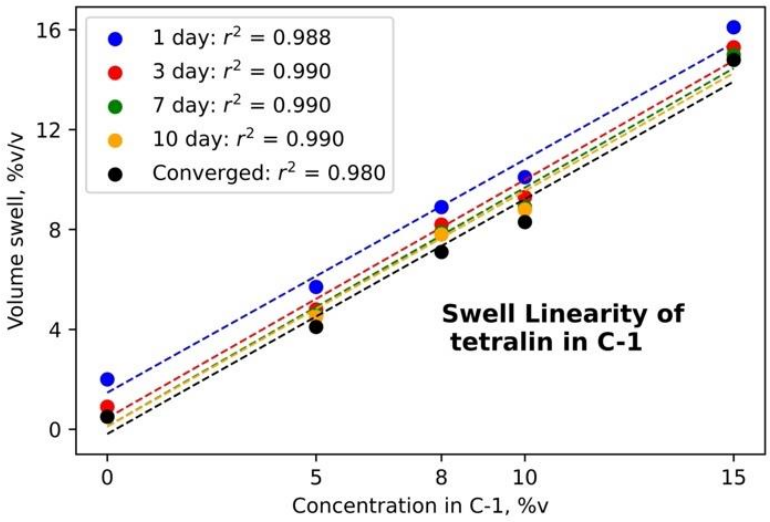

(c)

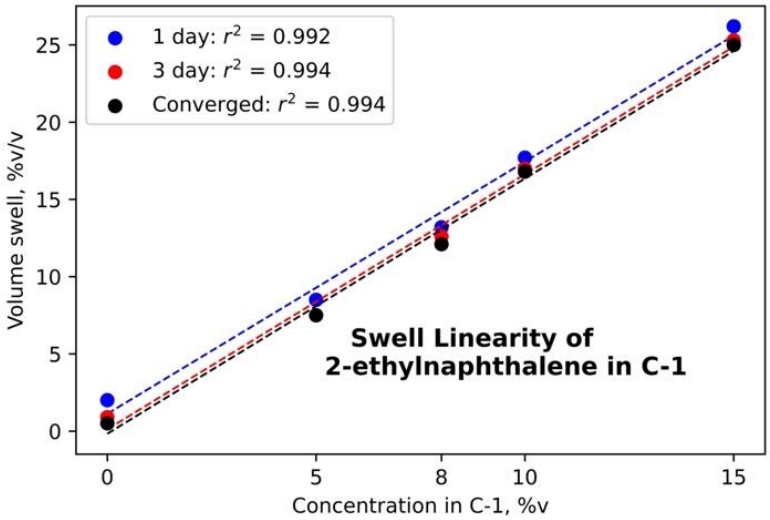

(d)

Figure 8: Scatter plots presenting the swell of 4 different dopants in C-1 at different concentrations. Each color marker and trendline represents the swell at a different timestep during the test.

All linear trendlines resulted in an r^2 of 0.92 or higher, indicating that the linear blending rule proposed in Kosir et al. [21] is likely suitable to predict the seal swell caused by aromatic molecules. While still useful for predictions, n-butylcyclohexane has a noticeably lower r^2 value than the rest of the dopants. This appears to be a result of some decay in swelling at higher concentrations and may indicate a limit to paraffin's contribution to seal swell. Future studies will verify this for similar dopants and/or fuel.

Also notable from this blending rule study is the comparative linearity for the mixtures at each timestep. For all intents and purposes, every molecule tested in this section shows approximately the same swell linearity and slope at all timesteps. This provides the

opportunity to estimate converged seal swell at any blend ratio based on one converged measurement and a series of measurements taken one day into the experiment. Any such estimate should always be confirmed with actual data, but this preliminary information informs test matrices and fuel development planning in far less time than the duration of a converged seal swell measurement. Advancements in swell projections of this manner may eventually lead to a feasible opportunity to include this testing methodology into the regulatory process.

3.6. Development of potential SAF swell blends

To demonstrate the application of the linear blending rule and the use of property relationships for molecule selection, four simple fuel mixtures were tested to compare with predicted values for several properties of interest, including seal swell, TSI, density, and dielectric constant. These blends were designed to meet the minimum density specification (775 kg/m3) and employed HEFA as the primary component with dopants of varying TSI to explore the tradeoff between seal swell and sooting propensity. Table 4 lists the developed blends, and the four plots in this section show the comparison between each mixture's predicted property values based on literature blending rules and the experimental results. Testing all four properties listed here required 25mL blends of each mixture.

All but one blend is predicted to be within conventional or specification range of seal swell (9.2-16.6%v/v) and dielectric constant (2.058077-2.119645) while exhibiting a lower TSI compared to conventional fuels (~22). The propylcyclohexane/trans-decalin doped blend is the exception to this, as an example of a possible zero-aromatic fuel and is not predicted to fall inside of the conventional dielectric constant range. While not comprehensive, the purpose of this exercise is to demonstrate the potential for implementation of o-ring volume swell prediction into the SAF prescreening process for all fuel properties described in Yang et al. [32]. The results of this exercise are shown below in Fig. 9.

Table 4: Predicted properties for SAF blends developed from Excel model

Blend Components	Blend Ratio (%v)	Projected Swell (%v/v)	Projected Density (kg/m^3)	Projected TSI	Projected DI
propylbenzene/propylcyclohexane/HEFA	20/9.58/70.41	15.6	775.2	14.4	2.06192
trans-decalin/indane/HEFA	4/10.42/85.58	11.9	775.3	10.2	2.05816
ethylbenzene/propylcyclohexane/HEFA	4.95/45.71/49.34	14.9	774.9	7.6	2.05844
1-methylnaphthalene/trans-decalin/HEFA	4/13.40/82.60	10.7	775.3	7.1	2.04912
propylcyclohexane/trans-decalin/HEFA	40/7.24/52.76	11.5	775.2	5.6	2.04480

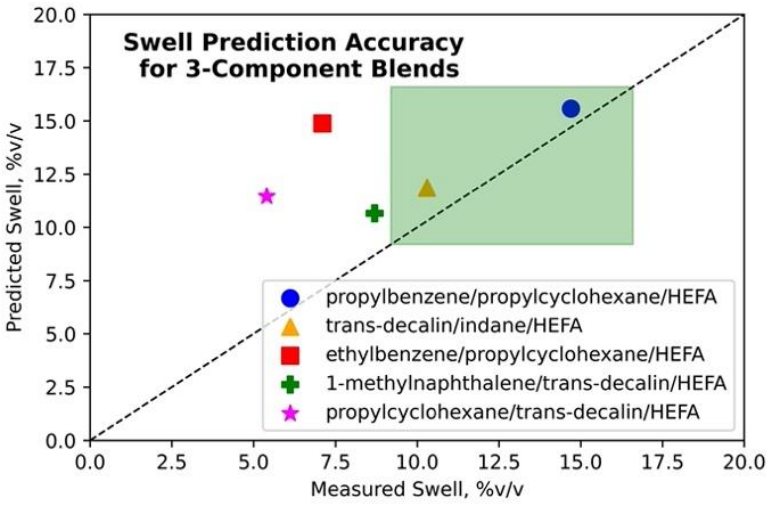
Swell Prediction Accuracy
for 3-Component Blends
Predicted Swell, %v/v
Measured Swell, %v/v
propylbenzene/propylcyclohexane/HEFA
trans-decalin/indane/HEFA
ethylbenzene/propylcyclohexane/HEFA
1-methylnaphthalene/trans-decalin/HEFA
propylcyclohexane/trans-decalin/HEFA
0.0
2.5
5.0
7.5
10.0
12.5
15.0
17.5
20.0

(a)

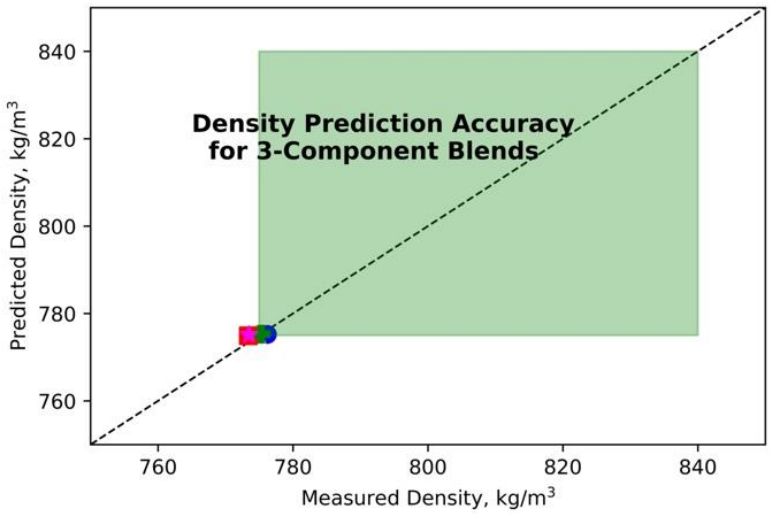
Density Prediction Accuracy
for 3-Component Blends
Predicted Density, kg/m³
Measured Density, kg/m³
760
780
800
820
840

(b)

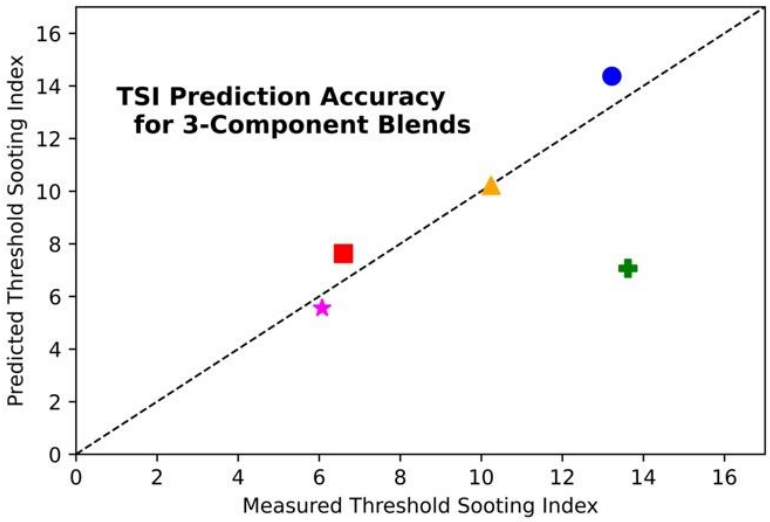

(c)

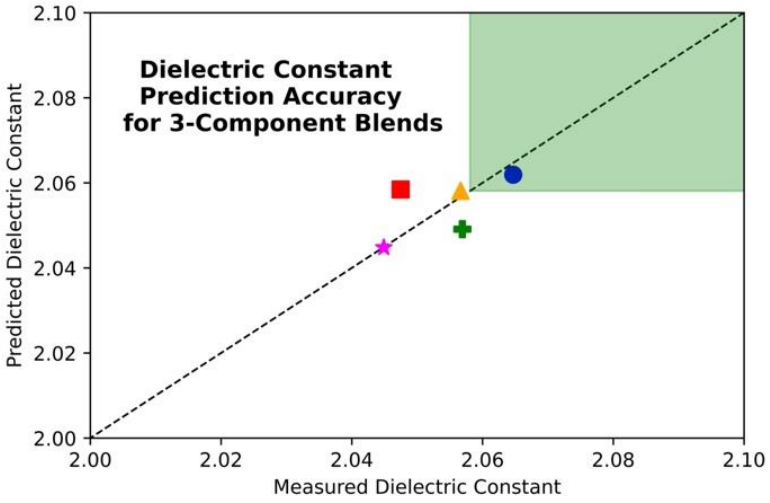

(d)

Figure 9: Unity plots for SAF swell blends with predicted and measured values. The green rectangles represent the conventional or specification range for the given property.

Only two of the blends achieved seal swell measured within conventional range. These blends held in common relatively low cycloparaffin content and depended on aromatics to induce sufficient seal swell. Two of the blends that failed to meet conventional o-ring swell had nearly 50%v cycloparaffin content, indicating that the slight decay in swell for n-butylcyclohexane at high concentrations may be generally true for cycloparaffins, but this requires verification via additional testing. The 1-methylnaphthalene/trans-decalin blend also failed to induce sufficient swell, making the possibility for small amounts of naphthalenes to induce desired swell without severely impacting emissions seem less likely.

While seal swell is the prominent focus of this work, the development of 100% drop-in SAF requires meeting specifications for many properties while maintaining lower emissions than petroleum fuels. All of the blends tested here measured below 15 TSI and roughly meet the minimum density specification. However, only the propylbenzene/propylcyclohexane blend met dielectric constant requirements, indicating that this property still requires special attention by fuel developers. Though these results do not consider all fuel properties, they represent choices that SAF developers can make to achieve material compatibility and imply that pathways utilizing some aromatics to induce seal swell are currently feasible without a dramatic impact on emissions. Further study is required to determine if zero-aromatic SAF is realistic but given the minimal TSI accomplished by the propylcyclohexane/trans-decalin blend presented here it should remain a goal of the community.

4. Conclusions and Future Work

Material compatibility with elastomer o-rings in fuel systems is currently one of the main limiting factors keeping SAF from 100% drop-in compatibility with existing fuel systems. To address this and ultimately reduce the commercial aviation sector's contribution to GHG emissions, the work presented here investigates o-ring swelling as it relates to fuel properties and a linear blending rule proposed in previous literature using optical dilatometry measurements. First, eight molecules were used in a small study to try and characterize the steric effects of aviation hydrocarbons on seal swell. Ultimately, these tests did not reveal a great deal about the nature of o-ring swelling but did find that even mixtures above the 8%v aromatic content called for by regulations did not guarantee swelling at conventional levels. This study also investigated the linear blending rule, albeit only at several concentrations up to 15%v in C-1. Two common elastomers used in aviation o-ring seals, fluorosilicone and nitrile rubber, were studied for blending and showed general adherence to the proposed rule, though fluorosilicone o-ring swell appeared more difficult to predict. This smaller study was used to inform and motivate a larger investigation and advance the testing capabilities of the project.

Using a much wider range of molecules, seal swell was measured and compared to the solvent's molar volume and density. Here it was found that the negative relationship between molar volume and o-ring swell holds true within hydrocarbon classes, but that density is a more suitable property to characterize swell generally over the mixtures tested. Like in the initial investigation, 8%v aromatic content did not consistently induce seal swell at the desired level, so it is recommended that actual seal swell measurements be used to assess material compatibility. The heated optical dilatometry method used in this work presents a potential pathway for these measurements, especially if future testing can be shortened even further without compromising the accuracy of results. The blending rule was also examined for higher concentrations of dopants in mixtures for nitrile rubber, showing a linear relationship generally suitable for swell prediction. Noted, however, was

an apparent decay in swelling propensity from cycloparaffins at high concentrations. Finally, the practical application of these findings was shown via a simple model to try and develop SAF blends with drop-in capability for density, seal swell, and dielectric constant while maintaining a TSI below that of conventional fuel. This demonstration was a relative success, with two out of five blends meeting swell conventional range and one meeting the other desired requirements. From this, the study currently recommends the usage of some aromatics in SAF for material compatibility, however zero-aromatic fuel remains the goal for the future.

The results of this study will guide future endeavors to further characterize the nature of o-ring swelling. Advanced modeling techniques using the data gathered here will provide further insight on what other properties associated with o-ring swell, such as Hansen Solubility Parameters, to investigate via testing. The blending rule will be investigated with more cycloparaffins to determine if the reduced swelling effect apparent at high concentrations is consistent across the class of hydrocarbons. Additionally, more complex blends will be studied to determine interaction effects between blend components on seal swell for both property relationships and blending rule. The results of this may reveal why several of the blends in this study did not achieve the swelling predicted by the linear blending rule. Eventually, the goal will be to understand the basic nature of seal swell and to use that information to accurately predict whether or not novel SAF can be considered material compatible. Beyond its usefulness in guiding future research, this study presently provides value in its measurements of many aviation hydrocarbons and analysis directly relevant to the work SAF developers in the industry.

Appendix A

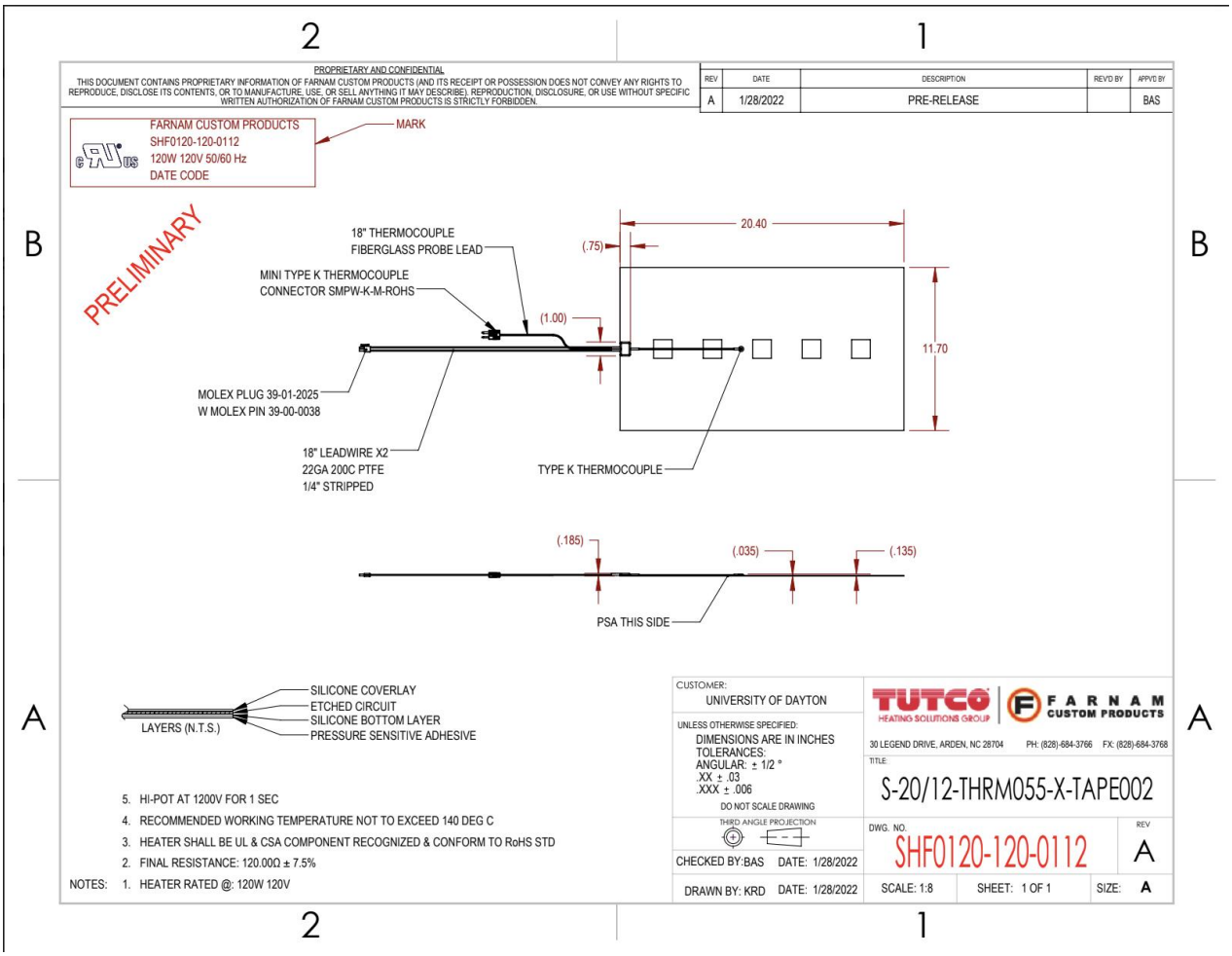

References

[1] "Mitigation of Climate Change Climate Change 2022 Working Group III contribution to the Sixth Assessment Report of the Intergovernmental Panel on Climate Change." [Online]. Available: https://www.ipcc.ch/site/assets/uploads/2018/05/uncertainty-guidance-note.pdf.

[2] "NIE_Climate_Change_and_National_Security".

[3] Nceh, "PREPARING FOR THE REGIONAL HEALTH IMPACTS OF CLIMATE CHANGE IN THE UNITED STATES." [Online]. Available: https://www.cdc.gov/climateandhealth/

[4] A. Beschloss and M. Mashayekhi, "The Economics of Climate Change – IMF F&D | December 2019." [Online]. Available: www.imf.org/fandd

[5] U. Epa, "CLIMATE CHANGE AND SOCIAL VULNERABILITY IN THE UNITED STATES A Focus on Six Impacts 2 Climate Change and Social Vulnerability in the

United States: A Focus on Six Impacts FRONT MATTER Acknowledgments." [Online]. Available: www.epa.gov/cira/technical-appendices-and-data.

[6] Habiba. Gitay and Intergovernmental Panel on Climate Change., *Climate change and biodiversity*. Intergovernmental Panel on Climate Change, 2002.

[7] "FACT SHEET: President Biden Sets 2030 Greenhouse Gas Pollution Reduction Target Aimed at Creating Good-Paying Union Jobs and Securing U.S. Leadership on Clean Energy Technologies," *White House Briefing Room*, Apr. 22, 2021. https://www.whitehouse.gov/briefing-room/statements-releases/2021/04/22/fact-sheet-president-biden-sets-2030-greenhouse-gas-pollution-reduction-target-aimed-at-creating-good-paying-union-jobs-and-securing-u-s-leadership-on-clean-energy-technologies/ (accessed Nov. 21, 2022).

[8] U. Epa and C. Change Division, "Inventory of U.S. Greenhouse Gas Emissions and Sinks: 1990-2020 – Main Text," 1990. [Online]. Available: https://www.epa.gov/ghgemissions/draft-inventory-us-greenhouse-gas-emissions-

[9] W. Schlenker *et al.*, "Airports, Air Pollution, and Contemporaneous Health," 2011. [Online]. Available: http://www.nber.org/papers/w17684

[10] N. Hudda, L. W. Durant, S. A. Fruin, and J. L. Durant, "Impacts of Aviation Emissions on Near-Airport Residential Air Quality," *Environ Sci Technol*, vol. 54, no. 14, pp. 8580–8588, Jul. 2020, doi: 10.1021/acs.est.0c01859.

[11] "Balancing growth in connectivity with a comprehensive global air transport response to the climate emergency: a vision of net-zero aviation by mid-century." [Online]. Available: www.bluesky-d2d.com

[12] "SAF Grand Challenge Roadmap Flight Plan for Sustainable Aviation Fuel."

[13] S. Kramer, G. Andac, J. Heyne, J. Ellsworth, P. Herzig, and K. C. Lewis, "Perspectives on Fully Synthesized Sustainable Aviation Fuels: Direction and Opportunities," *Frontiers in Energy Research*, vol. 9. Frontiers Media S.A., Jan. 24, 2022. doi: 10.3389/fenrg.2021.782823.

[14] "Designation: D4054 − 22 Standard Practice for Evaluation of New Aviation Turbine Fuels and Fuel Additives 1", doi: 10.1520/D4054-22.

[15] "Designation: D7566 − 22a Standard Specification for Aviation Turbine Fuel Containing Synthesized Hydrocarbons 1", doi: 10.1520/D7566-22A.

[16] D. S. Lee *et al.*, "The contribution of global aviation to anthropogenic climate forcing for 2000 to 2018," *Atmos Environ*, vol. 244, Jan. 2021, doi: 10.1016/j.atmosenv.2020.117834.

[17] C. Voigt *et al.*, "Cleaner burning aviation fuels can reduce contrail cloudiness," *Commun Earth Environ*, vol. 2, no. 1, p. 114, Dec. 2021, doi: 10.1038/s43247-021-00174-y.

[18] M. Romanczyk *et al.*, "The capability of organic compounds to swell acrylonitrile butadiene O-rings and their effects on O-ring mechanical properties," *Fuel*, vol. 238, pp. 483–492, Feb. 2019, doi: 10.1016/j.fuel.2018.10.103.

[19] Y. Liu and C. W. Wilson, “Investigation into the impact of n-decane, decalin, and isoparaffinic solvent on elastomeric sealing materials,” *Advances in Mechanical Engineering*, vol. 2012, 2012, doi: 10.1155/2012/127430.

[20] J. L. Graham, R. C. Striebich, K. J. Myers, D. K. Minus, and W. E. Harrison, “Swelling of nitrile rubber by selected aromatics blended in a synthetic jet fuel,” *Energy and Fuels*, vol. 20, no. 2, pp. 759–765, Mar. 2006, doi: 10.1021/ef050191x.

[21] S. Kosir, J. Heyne, and J. Graham, “A machine learning framework for drop-in volume swell characteristics of sustainable aviation fuel,” *Fuel*, vol. 274, Aug. 2020, doi: 10.1016/j.fuel.2020.117832.

[22] R. C. Boehm, Z. Yang, and J. S. Heyne, “Threshold Sooting Index of Sustainable Aviation Fuel Candidates from Composition Input Alone: Progress toward Uncertainty Quantification,” *Energy and Fuels*, vol. 36, no. 4, pp. 1916–1928, Feb. 2022, doi: 10.1021/acs.energyfuels.1c03794.

[23] “World’s first passenger flight with 100% renewable fuel takes off—thanks to biotech | BIO.” https://www.bio.org/blogs/worlds-first-passenger-flight-100- renewable-fuel-takes-thanks-biotech (accessed Nov. 21, 2022).

[24] J. Feldhausen, D. C. Bell, Z. Yang, C. Faulhaber, R. Boehm, and J. Heyne, “Synthetic aromatic kerosene property prediction improvements with isomer specific characterization via GCxGC and vacuum ultraviolet spectroscopy,” *Fuel*, vol. 326, p. 125002, Oct. 2022, doi: 10.1016/j.fuel.2022.125002.

[25] A. Anuar, V. K. Undavalli, B. Khandelwal, and S. Blakey, “Effect of fuels, aromatics and preparation methods on seal swell,” *Aeronautical Journal*, vol. 125, no. 1291, pp. 1542–1565, Sep. 2021, doi: 10.1017/aer.2021.25.

[26] T. Rahmes, “Impact of Alternative Jet Fuel and Fuel Blends on Non-Metallic Materials Used in Commercial Aircraft Fuel Systems Continuous Lower Energy, Emissions and Noise (CLEEN) Program.”

[27] “Seals for Alternative Fuels”.

[28] M. Colket *et al.*, “Overview of the national jet fuels combustion program,” in *AIAA Journal*, 2017, vol. 55, no. 4, pp. 1087–1104. doi: 10.2514/1.J055361.

[29] “ImageJ Wiki.” https://imagej.net/ (accessed Nov. 21, 2022).

[30] “ImageJ Homepage,” *National Intstitute of Health*. https://imagej.nih.gov/ij/ (accessed Nov. 21, 2022).

[31] “PQIS 2011”.

[32] Z. Yang, S. Kosir, R. Stachler, L. Shafer, C. Anderson, and J. S. Heyne, “A GC × GC Tier α combustor operability prescreening method for sustainable aviation fuel candidates,” *Fuel*, vol. 292, 2021, doi: 10.1016/j.fuel.2021.120345.